NANO LETTERS
Cite This: Nano Lett. XXXX, XXX, XXX−XXX
Letter
pubs.acs.org/NanoLett

Dielectric Engineering of Electronic Correlations in a van der Waals Heterostructure

Philipp Steinleitner,[†] Philipp Merkl,[†] Alexander Graf,[†] Philipp Nagler,[†] Kenji Watanabe,[‡] Takashi Taniguchi,[‡] Jonas Zipfel,[†] Christian Schüller,[†] Tobias Korn,[†] Alexey Chernikov,[†] Samuel Brem,[§] Malte Selig,[∥] Gunnar Berghäuser,[§] Ermin Malic,*[,§] and Rupert Huber*[,†]

[†]Department of Physics, University of Regensburg, Universitätsstraße 31, 93053 Regensburg, Germany
[‡]National Institute for Material Science, 305-0044 1-1 Namiki Tsukuba, Ibaraki, Japan
[§]Department of Physics, Chalmers University of Technology, Fysikgården 1, 41258 Gothenburg, Sweden
[∥]Department of Theoretical Physics, Technical University of Berlin, Hardenbergstraße 36, 10623 Berlin, Germany

Supporting Information

ABSTRACT: Heterostructures of van der Waals bonded layered materials offer unique means to tailor dielectric screening with atomic-layer precision, opening a fertile field of fundamental research. The optical analyses used so far have relied on interband spectroscopy. Here we demonstrate how a capping layer of hexagonal boron nitride (hBN) renormalizes the internal structure of excitons in a WSe_2 monolayer using intraband transitions. Ultrabroadband terahertz probes sensitively map out the full complex-valued mid-infrared conductivity of the heterostructure after optical injection of 1s A excitons. This approach allows us to trace the energies and line widths of the atom-like 1s−2p transition of optically bright and dark excitons as well as the densities of these quasiparticles. The excitonic resonance red shifts and narrows in the WSe_2/hBN heterostructure compared to the bare monolayer. Furthermore, the ultrafast temporal evolution of the mid-infrared response function evidences the formation of optically dark excitons from an initial bright population. Our results provide key insight into the effect of nonlocal screening on electron−hole correlations and open new possibilities of dielectric engineering of van der Waals heterostructures.

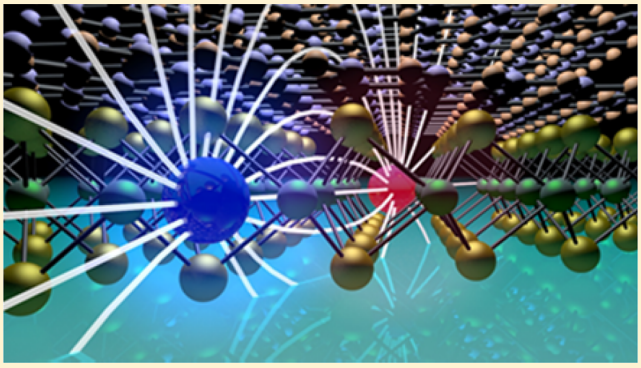

KEYWORDS: *Dichalcogenides, atomically thin 2D crystals, van der Waals heterostructures, dielectric engineering, dark excitons.*

Atomically thin layers of transition metal dichalcogenides (TMDCs) have been in the spotlight of physical and chemical research due to a unique combination of properties. In particular, TMDC monolayers exhibit a direct energy gap in the optical range[1,2] in sharp contrast to gapless graphene, which makes them fascinating candidates for ultimately thin optoelectronic devices.[3−5] Interestingly, the electronic and optical properties of this material system are dominated by Coulomb-bound electron−hole pairs, called excitons,[6,7] rather than by unbound charge carriers. Reduced Coulomb screening in combination with the reduced dimensionality of atomically thin crystals leads to a dramatic increase of the exciton binding energy to typical values of few hundred millielectronvolts, stabilizing these states even at room temperature.[7−13] Owing to the extreme confinement perpendicular to the plane of the material, excitons are particularly sensitive to the local environment surrounding the monolayer.[14−22] The possibility to vertically stack different cover materials onto two-dimensional TMDCs[4,23] has thus opened an exciting platform for fundamental physics[20,24−32] and device technologies.[33,34] On the one hand, heterostructures consisting of two different semiconducting monolayers have been employed to realize ultrathin p−n junctions[33] and interlayer excitons[24,26,35] due to the possibility of interlayer charge transfer.[24,26,33,35] On the other hand, TMDC monolayers covered with an insulating van der Waals material have allowed for a less invasive strategy of Coulomb engineering.[17,20] By dielectric sculpting of the electric field lines connecting electrons and holes, in-plane electronic correlations can be modified within the TMDC monolayer without changing the chemical structure of the material itself.[20] Electron−phonon interactions[30,31,36,37] may be controlled and in-plane heterostructures can be realized on a nanometer length scale.[17,20]

The most widespread methods of investigating excitons probe their interband generation or annihilation.[7,10,11] In these experiments, light couples dominantly to only a minor fraction of excitons, namely the optically bright ones. Optically dark states, whose interband dipole moment vanishes or whose

Received: December 6, 2017
Revised: January 19, 2018
Published: January 24, 2018

DOI: 10.1021/acs.nanolett.7b05132
Nano Lett. XXXX, XXX, XXX−XXX

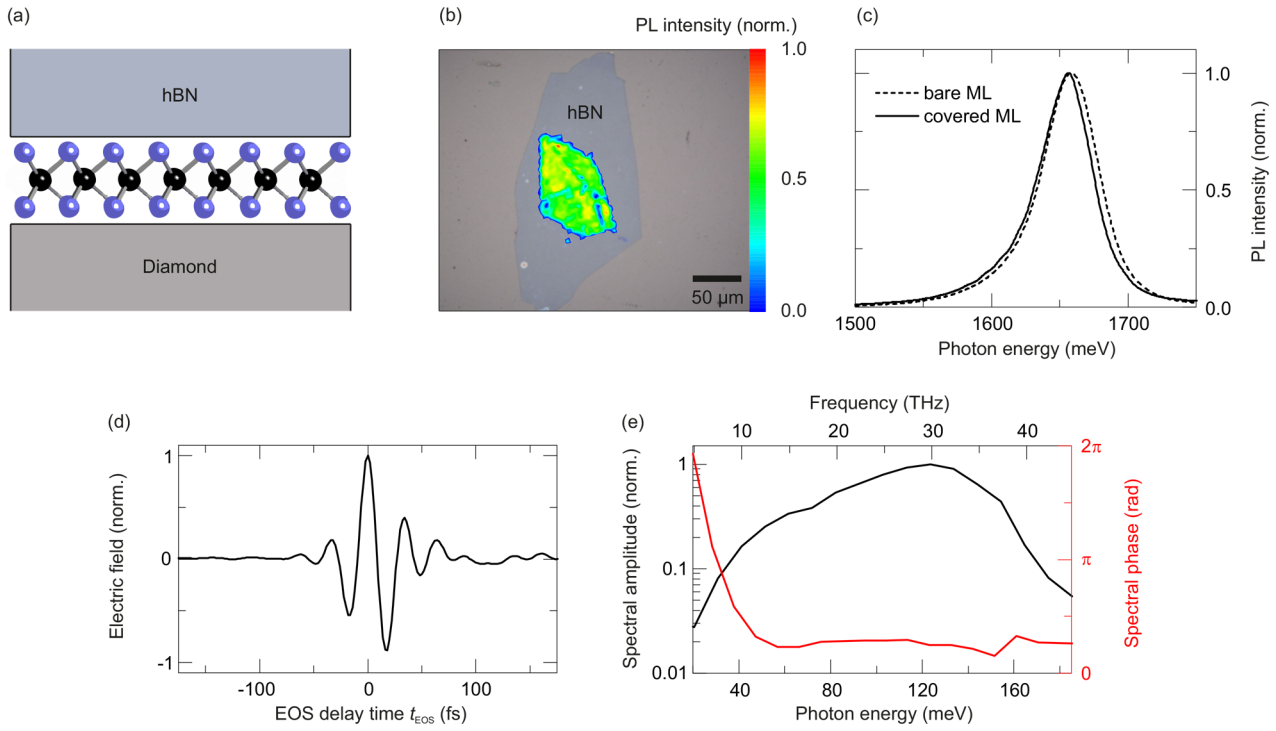

Figure 1. (a) Artist's view of the sample structure. A WSe_2 monolayer (blue and black spheres) on a CVD diamond window is covered with a capping layer of hexagonal boron nitride (hBN, thickness: 100 nm). The WSe_2/hBN heterostructure is fabricated by mechanical exfoliation of the individual components and subsequent deterministic transfer from a viscoelastic substrate onto a CVD diamond substrate. (b) Optical microscopy image and room-temperature PL intensity map of the WSe_2/hBN heterostructure excited by a continuous-wave laser at a wavelength of 532 nm. The lateral dimensions of the WSe_2 monolayer are about 100 μm × 75 μm. (c) Corresponding PL intensity spectrum (black solid curve) compared to the PL spectrum of a bare monolayer (black dashed curve). (d) Waveform of the phase-stable single-cycle mid-IR probe pulse E_{ref} transmitted through the unexcited heterostructure as a function of the electro-optic gate delay time t_{EOS}. (e) Corresponding multioctave spanning amplitude (black curve) and phase spectrum (red curve) as obtained by Fourier transformation of $E_{ref}(t_{EOS})$.

center-of-mass momenta lie outside the light cone, cannot be directly addressed this way and have required more sophisticated in-plane propagation geometries[38] or phonon-assisted processes.[37] Mid-infrared (mid-IR) photons, in contrast, may directly induce a hydrogen-like 1s−2p transition in pre-existing species, irrespective of interband dipole moments and large center-of-mass momenta. This concept has been employed to explore the formation time and dynamics of excitons in TMDC monolayers[12,13,39,40] and also represents a promising tool for the investigation of electronic correlations in heterostructures. Still, the direct influence of a cover layer on the correlations between orbital states of excitons has not been resolved in a direct, resonant way.

In this Letter, we experimentally investigate the influence of an insulating hexagonal boron nitride cover layer on the fundamental intraexcitonic 1s−2p resonance by the absorption of mid-IR photons in the TMDC monolayer WSe_2. By utilizing intraband spectroscopy, we are able to address all excitons in the system, including bright and dark states. This approach allows us to reveal the influence of the cover layer and its dielectric constant on the internal structure of excitons in the most direct possible way. We find that an hBN cover layer leads to a significant renormalization of the intraexcitonic 1s−2p transition by 23 meV and a decrease of the transition line width compared to the uncovered monolayer. Moreover, the ultrafast evolution of the mid-IR response functions shows a distinct blue shift of the intraexcitonic 1s−2p resonance transition and an increase of its line width with time. Using microscopic modeling, we show that these observations are characteristic of the formation of dark excitons from the initial bright population.

The WSe_2/hBN heterostructure (Figure 1a) is manufactured by mechanical exfoliation and van der Waals bonding.[41] First, a monolayer of WSe_2 is deterministically transferred from a viscoelastic substrate onto a CVD diamond window. Subsequently, the cover layer is added onto the monolayer in the same way. The homogeneous distribution of the photoluminescence (PL) intensity across the WSe_2 flake (Figure 1b) confirms the structural integrity of the monolayer after being covered with hexagonal boron nitride. Furthermore, the corresponding PL intensity spectrum (Figure 1c, black solid curve) features a peak energy of 1656 meV and a line width of 47 meV (fwhm). A comparison of these values to a PL spectrum of an uncovered monolayer (Figure 1c, black dashed curve) shows that covering reduces the line width of the PL by 5%, but hardly affects its spectral position. These observations are in line with recent interband spectroscopy results.[18−20,22,35] The thickness of the hBN cover layer is 100 nm, measured with atomic force microscopy.

To explore the influence of the capping layer on the electronic correlations in the WSe_2 monolayer, especially the fundamental intraexcitonic transition, we resonantly create bright 1s A excitons[12] by optical excitation with a 100 fs laser pulse centered at a wavelength of 745 nm (1664 meV, Supporting Information Figure S1). The pump fluence is set to Φ = 27 μJ/cm^2 in order to keep the excitation density at a moderate level.[40] For the direct observation of the hydrogen-like 1s−2p transition of the injected excitons, we use phase-

DOI: 10.1021/acs.nanolett.7b05132
Nano Lett. XXXX, XXX, XXX−XXX

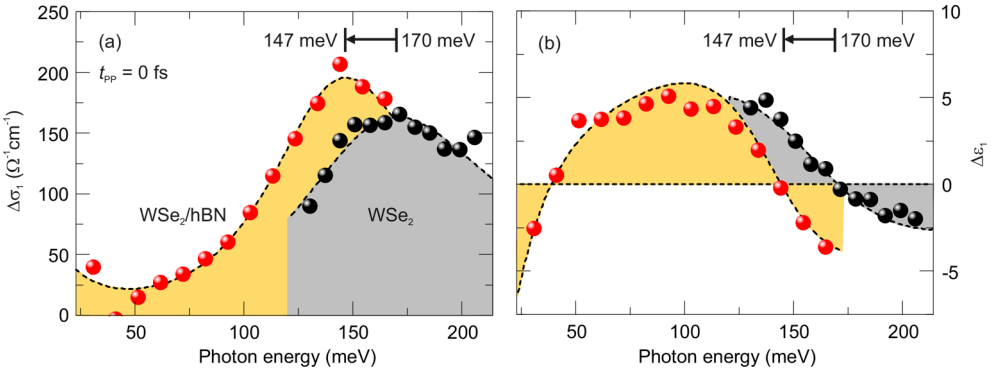

Figure 2. Pump-induced changes of the real parts of the optical conductivity $\Delta\sigma_1$ (a) and the dielectric function $\Delta\varepsilon_1$ (b) as a function of the photon energy, for a fixed pump delay time t_{PP} = 0 fs after resonant excitation. The red spheres (yellow shading) denote the experimental data of the photoexcited WSe_2/hBN heterostructure (pump fluence Φ = 27 μJ/cm^2), whereas the black spheres (gray shading) describe the experimental data of a photoexcited monolayer (pump fluence Φ = 25 μJ/cm^2, taken from ref 12). The black dashed curves represent the results by a phenomenological Drude–Lorentz model (eq 1) fitting simultaneously $\Delta\sigma_1$ and $\Delta\varepsilon_1$. This model takes unbound electron–hole pairs as well as excitons into account.[13] The arrows indicate the shift of the resonance from 170 meV (bare monolayer) to 147 meV (hBN covered monolayer).

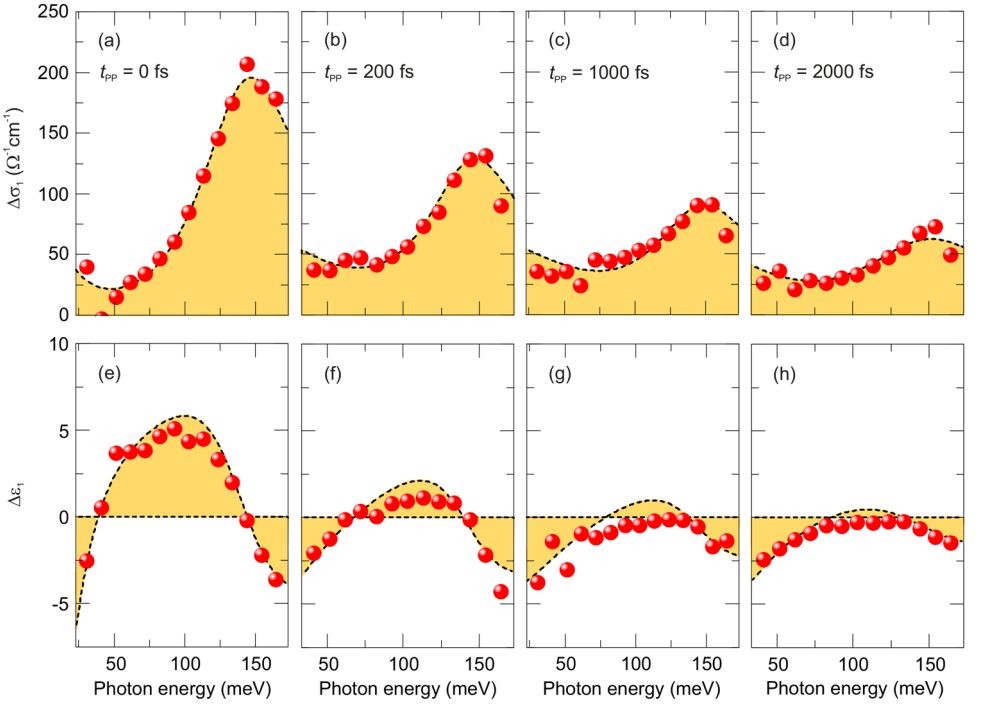

Figure 3. Pump-induced changes of the real parts of the optical conductivity $\Delta\sigma_1$ (a–d) and the dielectric function $\Delta\varepsilon_1$ (e–h) as a function of the photon energy, for several pump delay times t_{PP} after resonant excitation. The red spheres (yellow shading) denote the experimental data of the photoexcited WSe_2/hBN heterostructure (pump fluence Φ = 27 μJ/cm^2). The black dashed curves represent the results of a phenomenological Drude–Lorentz model (eq 1) fitting simultaneously $\Delta\sigma_1$ and $\Delta\varepsilon_1$.

locked single-cycle mid-IR pulses (Figure 1d) generated by optical rectification of the fundamental laser output in a 10-μm-thin GaSe crystal. The pulses feature a flat spectral phase (Figure 1e, red curve) throughout their multioctave spanning amplitude spectrum ranging from photon energies between 30 and 165 meV (Figure 1e, black curve). By electro-optic sampling up to the mid-IR spectral region, the absolute amplitude and phase of the transmitted electric field waveform $E_{ref}(t_{EOS})$ are recorded as a function of the detection time t_{EOS}. We compare the mid-IR probe transient through the excited and the unexcited sample and determine the pump-induced change $\Delta E(t_{EOS})$ for a given delay time t_{PP} between pumping and probing. The amplitude of ΔE is typically on the order of a few times 10^{-3} compared to the peak of E_{ref}. A continuous variation of t_{PP} provides access to the ultrafast dynamics of the nonequilibrium system (Supporting Information Figure S2). All experiments are performed at room temperature and ambient conditions.

From the quantities $E_{ref}(t_{EOS})$ and $\Delta E(t_{EOS}, t_{PP})$ the complex-valued mid-IR response function of the resonantly excited heterostructure can be extracted via a transfer matrix formalism.[42,43] The mid-IR response function includes the change in the real parts of the mid-IR conductivity ($\Delta\sigma_1$) and the dielectric function ($\Delta\varepsilon_1$), roughly corresponding to absorptive and inductive components, respectively. The advantage of the field-sensitive detection is that both functions can be extracted independently, without resorting to a Kramers–Kronig analysis.

DOI: 10.1021/acs.nanolett.7b05132
Nano Lett. XXXX, XXX, XXX–XXX

Figure 2 compares the mid-IR response ($\Delta\sigma_1$ and $\Delta\varepsilon_1$) of the WSe_2/hBN heterostructure and a bare uncovered monolayer for a pump delay time of t_{PP} = 0 fs. In the case of the bare monolayer (Figure 2a,b, gray shading), a peak in $\Delta\sigma_1$ and a corresponding zero crossing in $\Delta\varepsilon_1$ around an energy of 170 meV are observed. These features are characteristic of a resonant absorption and can be assigned to the 1s−2p transition of excitons in this system.[12,13] In the case of the heterostructure (Figure 2a,b, yellow shading), we find a similar spectral shape. However, the characteristic peak in $\Delta\sigma_1$ and the zero crossing in $\Delta\varepsilon_1$ are now located at a distinctly lower energy of 147 meV while the resonance is notably narrower. We will show below that these features originate from the renormalized 1s−2p transition of the resonantly generated excitons.

The nature of the screened excitons also manifests itself in their dynamics. Figure 3 displays the ultrafast evolution of the mid-IR response of the WSe_2/hBN heterostructure for a series of delay times t_{PP}. Compared to the response at t_{PP} = 0 fs (Figure 3a,e), the overall magnitude of the signal decreases, the resonance blue shifts slightly and the line width broadens as a function of t_{PP} (Figure 3b−d,f−h). Interestingly, a second zero crossing in $\Delta\varepsilon_1$ persists on the low-frequency end of the spectral window for all pump delay times t_{PP}. This feature may be caused by a second low-energy resonant absorption or by unbound electron−hole pairs, whose contribution would have a similar effect on $\Delta\varepsilon_1$.

For a more quantitative evaluation of the measured mid-IR response functions (Figures 2 and 3), we apply a Drude−Lorentz model[13,44,45] reflecting the contribution of excitons (Lorentz) and an electron−hole plasma (Drude) on a phenomenological level. Within this approach, pump-induced changes in the frequency-dependent dielectric function $\Delta\varepsilon(\omega) = \Delta\varepsilon_1 + i\Delta\sigma_1/(\varepsilon_0\omega)$ are described using two components

$$\Delta\varepsilon(\omega) = \frac{n_X e^2}{d\varepsilon_0\mu}\frac{f_{1s,2p}}{\frac{E_{res}^2}{\hbar^2} - \omega^2 - i\omega\Delta} - \frac{n_{FC}e^2}{d\varepsilon_0\mu}\frac{1}{\omega^2 + i\omega\Gamma} \quad (1)$$

The first term, a Lorentzian resonance, represents the intraexcitonic 1s−2p line. It includes the 1s exciton density n_X, the corresponding reduced mass $\mu = m_e m_h/(m_e+m_h)$ (m_e and m_h are the effective masses of the constituent electron and hole), the effective thickness d of the monolayer (treated as a thin slab in this model), the oscillator strength $f_{1s,2p}$ of the intraexcitonic transition, the resonance energy E_{res}, and the line width Δ. Additional constants are the electron charge e and the vacuum permittivity ε_0. The second term represents the Drude response of the electron−hole plasma, which depends on the density of free carriers n_{FC} and their scattering rate Γ. For the analysis of the data, we fix the reduced mass μ = 0.17 m_0 and the oscillator strength for the covered monolayer $f_{1s,2p}^{hetero} = 0.30$ ($f_{1s,2p}^{bare} = 0.32$ see ref 12), corresponding to electron−hole properties at the K and K′ valleys in WSe_2. The effective monolayer thickness d is set to 0.7 nm. The remaining parameters of the Drude−Lorentz model (n_X, n_{FC}, E_{res}, Δ, Γ) are extracted by fitting the experimental data. The fact that both independently measured $\Delta\sigma_1$ and $\Delta\varepsilon_1$ spectra need to be simultaneously reproduced poses strict limits on the possible values of the fitting parameters. The numerical adaptation (Figures 2 and 3, black dashed curves) yields an overall good fit quality. Note that this model has been well established for a phenomenological description of the intraexcitonic dielectric response,[12,13,44,45] yet it neglects Coulomb correlations between unbound charge carriers as well as higher-order correlations between carriers and excitons.[46] Furthermore, it accounts only for a single excitonic resonance. In reality, however, multiple spectrally overlapping excitonic resonances can emerge for pump delay times t_{PP} > 0 fs (see discussion below). Equation 1 would model overlapping transitions by an increased broadening Δ. Finally, excitonic resonances located far below the accessible spectral window yield a Drude-like contribution, which, in the framework of the above model, would be mimicked by the response of free carriers.

For the bare monolayer, the fitting procedure of the experimental data at a pump delay time t_{PP} = 0 fs (Figure 2a,b, black spheres) yields an exciton density of 3.63 × 10^{12} cm^{-2}, a resonance energy of 170 meV, and a line width of 117 meV. There is no measurable contribution from unbound electron−hole pairs in the investigated spectral region, in agreement with previous works.[12,13] In contrast, adding the hBN cover layer red shifts the resonance E_{res} to 147 meV, whereas the line width Δ decreases to 90 meV at t_{PP} = 0 fs (Figure 2a,b, red spheres). Furthermore, the fit of the heterostructure data reveals a nonvanishing density of unbound electron−hole pairs n_{FC}.

Figure 4 summarizes the complete temporal evolution of the fitting parameters n_X, n_{FC}, Δ and E_{res} for the WSe_2/hBN heterostructure. The density of excitons (Figure 4a, black spheres) initially decays within the first hundreds of femtoseconds from n_X = 3.93 × 10^{12} cm^{-2} to 2.15 × 10^{12} cm^{-2} followed by a much slower decay on a picosecond scale.[12] This dynamics corresponds to the radiative recombination of coherent bright excitons followed by the decay of incoherent dark states.[12,47] The pump-induced change ΔE observed at a fixed electro-optic sampling time t_{EOS} = 0 fs (Figure 4a, black solid line) has been established to be proportional to the exciton density.[12,13] Thus, recording $\Delta E(t_{EOS}$ = 0 fs) as a function of t_{PP} provides an alternative access to the temporal evolution of the exciton density. The almost perfect agreement of the temporal shape of $n_X(t_{PP})$ (Figure 4a, black spheres) with $\Delta E(t_{EOS}$ = 0 fs, $t_{PP})$ (Figure 4a, black solid line) further corroborates the phenomenological Drude−Lorentz model of eq 1.

The density of unbound electron−hole pairs n_{FC} (Figure 4a, red spheres) rises within the first 200 fs, starting from a nonvanishing value n_{FC} = 0.1 × 10^{12} cm^{-2}, and slowly decays on a much longer time scale. Furthermore, n_{FC} is an order of magnitude smaller than n_X for all pump delay times t_{PP}. As noted above, the effect of a finite plasma density may also indicate the presence of a Lorentzian line located below the spectral window accessed here and will be further investigated in future research. The temporal evolution of the resonance energy E_{res} is depicted in Figure 4b. Starting from an initial value of 147 meV at t_{PP} = 0 fs, E_{res} blue shifts up to 153 meV at t_{PP} = 2 ps. The line width Δ, however, decreases from 90 to 80 meV, within 200 fs, followed by a monotonic increase up to Δ = 112 meV at t_{PP} = 2 ps (Figure 4c).

Both the spectral response and its ultrafast evolution provide novel evidence of renormalized Coulomb correlations shaped by the dielectric screening, as we show next. To explain the pronounced red shift of the intraexcitonic 1s−2p transition energy of the heterostructure by 23 meV, we perform calculations on a microscopic level explicitly taking into account the dielectric constant of the surrounding diamond

DOI: 10.1021/acs.nanolett.7b05132
Nano Lett. XXXX, XXX, XXX−XXX

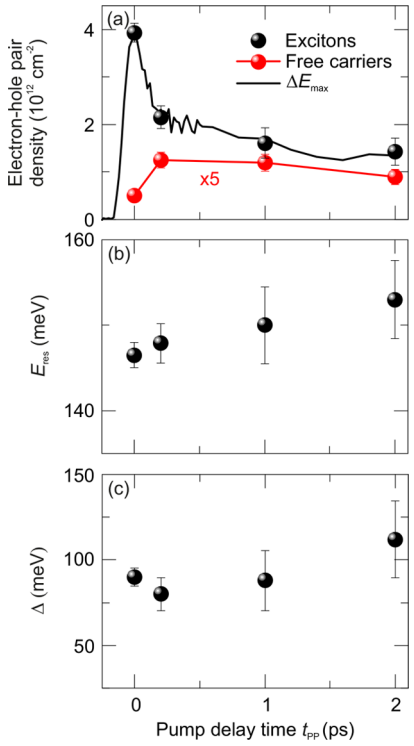

Figure 4. (a) Temporal evolution of the exciton density n_X (black spheres, excitons) and the unbound electron−hole pair density n_{FC} (red spheres, free carriers) as extracted from fitting the mid-IR response function of the WSe_2/hBN heterostructure (Figure 3, red spheres) measured for different pump delay times t_{PP} with the Drude-Lorentz model. The pump-induced change ΔE recorded at fixed electro-optic sampling time t_{EOS} = 0 fs (ΔE_{max}, black solid line) is proportional to the exciton density n_X. Resonance energy E_{res} (b) and line width Δ (c) as a function of the pump delay time t_{PP} as obtained from fitting the experimental mid-IR response data of the heterostructure (Figure 3, red spheres). The error bars represent the 95% confidence intervals of the fitting parameters.

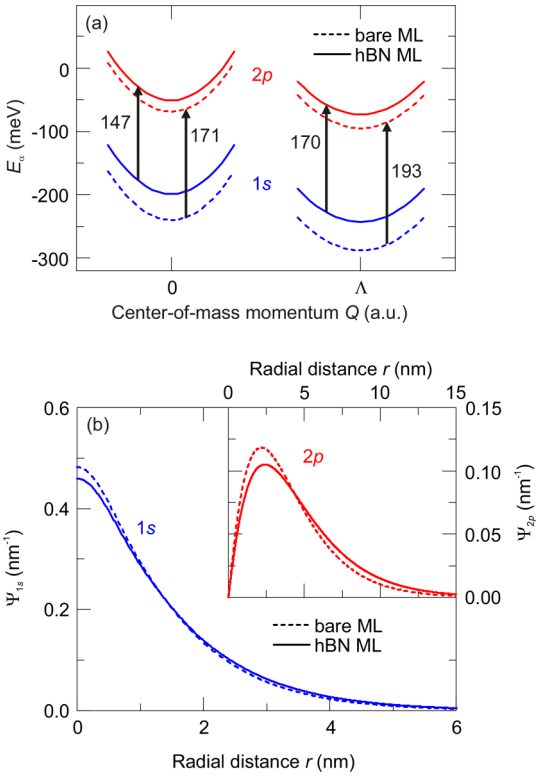

Figure 5. (a) Calculated binding energies E_α (α = 1s, 2p) for intravalley K−K excitons (parabolae around Q = 0) as well as momentum-forbidden dark K−Λ excitons (parabolae around Q = Λ) as a function of the center-of-mass momentum Q. The black arrows symbolize various intraexcitonic 1s−2p transitions. (b) Calculated radial wave functions $\Psi_\alpha(r)$ for the 1s (blue curves) and 2p (red curves) bright excitonic levels (Q = 0). The dashed lines are related to the bare monolayer, whereas the solid lines refer to calculations for the monolayer covered with hBN.

substrate and the hBN cover layer. In the case of the heterostructure, we expect increased screening of the Coulomb potential compared to the bare monolayer, which should result in a reduction of the binding energy of excitons and thus in a red shift of the 1s−2p transition energy. Solving the excitonic Wannier equation in momentum representation[36]

$$\frac{\hbar^2 q^2}{2\mu}\Psi_\alpha(q) - \sum_k V_{exc}(q, k)\Psi_\alpha(q + k) = E_\alpha \Psi_\alpha(q) \quad (2)$$

we have microscopic access to exciton binding energies E_α and wave functions $\Psi_\alpha(q)$ with index α = 1s, 2s, 2p, ... Here, we have introduced the excitonic part of the Coulomb interaction $V_{exc}(q, k)$, which is treated within the thin-film formalism for 2D systems.[8,9,14,48,49] The latter also contains the dielectric background screening $\varepsilon_{BG} = \frac{\varepsilon_{cover} + \varepsilon_{substrate}}{2}$ of the underlying substrate/cover layer.

Figure 5a shows the calculated binding energies of 1s and 2p states of intravalley K−K excitons (parabolae around Q = 0) as well as momentum-forbidden dark K-Λ excitons (parabolae around Q = Λ) as a function of the center-of-mass momentum Q. Broken (solid) curves indicate the situation for the bare (hBN covered) monolayer. The corresponding radial wave functions for bright excitons (Q = 0) are depicted in Figure 5b. We can perfectly reproduce the experimentally observed 1s−2p resonance energy of 147 meV at t_{PP} = 0 fs for bright K−K excitons with a dielectric constant of ε_{cover} = 2.3, which agrees well with the literature value for hBN.[50] Thus, we can unequivocally assign the observed resonance at 147 meV to the renormalized 1s−2p transition in the heterostructure.

The ultrafast evolution of the resonance energy E_{res} shows a monotonic blue shift with increasing pump delay time t_{PP} (Figure 4b). This feature can be explained by the formation of a momentum-forbidden dark intervalley exciton population via exciton−phonon scattering or the emergence of spin-unlike excitons due to spin-flip processes.[40] Since the intraexcitonic 1s−2p separation of dark K−Λ excitons is higher than the one of the initially bright excitons (Figure 5a), E_{res} increases as the dark population forms.[40] Furthermore, the dark excitonic ground state (Q = Λ) in WSe_2 is energetically lower than the bright one (Q = 0, Figure 5a) leading to an efficient accumulation of K−Λ excitons during thermalization.[40]

Next we turn to the strong reduction of the line width Δ from 117 meV for the bare monolayer to 90 meV for the heterostructure at t_{PP} = 0 fs. This fact appears even more striking when the corresponding exciton densities are considered. Δ is expected to increase with n_X.[12,13] In our experiment, the line width Δ_{hetero} is found to be smaller than Δ_{bare} by 23%, even though the density n_X^{hetero} slightly exceeds n_X^{bare} by 8%. Thus, the hBN cover layer clearly reduces the width of the intraexcitonic 1s−2p transition line. One of the possible broadening mechanisms contributing to the line width

DOI: 10.1021/acs.nanolett.7b05132
Nano Lett. XXXX, XXX, XXX−XXX

Δ is exciton−phonon scattering. Here, the scattering efficiency is i.a. determined by the overlap of excitonic wave functions.[36] Since stronger Coulomb screening, caused by the change of the dielectric environment, leads to more spatially extended exciton wave functions (Figure 5b), exciton−phonon scattering should be modified in the heterostructure. However, our numerical calculations reveal that in the relevant range of dielectric background constants ε_{BG}, the scattering with acoustic phonons is slightly enhanced by adding hBN, whereas the interaction with optical phonons becomes weaker, so that in total the exciton−phonon scattering is almost the same with and without hBN. Thus, this mechanism cannot cause the observed decrease of the line width Δ. Exciton−exciton scattering, however, depends on the Coulomb potential which is indirectly proportional to ε_{BG}. Thus, the increase of ε_{BG}, caused by adding a cover layer, can lead to a decrease of exciton−exciton scattering, resulting in a smaller line width Δ.

The temporal evolution of the line width (Figure 4c) shows another unexpected behavior. Δ should decrease as a function of t_{PP} because the overall electron−hole pair density decreases (Figure 4a as well as Supporting Information Figures S3 and S4) and thus fewer scattering events take place. However, the line width after an initial and expected decrease starts to rise from 80 meV at t_{PP} = 0.2 ps to 112 meV at t_{PP} = 2 ps. This anomalous behavior is a second indication for dark intervalley or spin-unlike excitons both having higher resonance energies than the bright states.[40] Because our mid-IR probe pulse is sensitive to all kinds of dark excitons, the superposition of various intraexcitonic 1s−2p absorption peaks from different momentum- or spin-forbidden states leads to an apparent increase of the line width, as the dark population (t_{PP} > 0.2 ps) forms from the initial bright exciton population (t_{PP} < 0.2 ps). Since the overall electron−hole pair density steadily decreases for t_{PP} > 0.2 ps (Figure 4a) and thus the line width Δ should show a similar trend, the observed strong blue shift of E_{res} can only be accounted for by the formation of dark excitons.[40]

In conclusion, intraband spectroscopy in the mid-IR spectral range allows us to investigate the influence of the modification of the dielectric environment on bright and dark excitons in a WSe_2 monolayer. The data quantify internal transition energies, densities and many-body effects. Most remarkably, we observe a significant red shift of the intraexcitonic 1s−2p transition as well as a decrease of its line width compared to the uncovered monolayer. Furthermore, the distinct blue shift of the 1s−2p resonance along with the anomalous dynamics of the line width suggests the formation of a dark exciton population from an initial bright one. These heterostructures fabricated by simple stacking offer an exciting playground to custom-tailor electronic correlations and thus open exciting perspectives for novel optoelectronic applications. In future studies yet sharper resonances may be achieved by full encapsulation of the monolayer with hBN.[19] Furthermore, one may even resonantly hybridize excitonic transitions with low-energy excitation of surrounding cover layers, designing novel material parameters by layer-sensitive dielectric sculpting.

■ ASSOCIATED CONTENT

Supporting Information

The Supporting Information is available free of charge on the ACS Publications website at DOI: 10.1021/acs.nanolett.7b05132.

Interband absorbance of the WSe_2/hBN heterostructure. Field-resolved optical pump/mid-infrared probe spectroscopy. Pump fluence dependence of the line width of the intraexcitonic 1s−2p transition (PDF)

■ AUTHOR INFORMATION

Corresponding Authors

*E-mail: ermin.malic@chalmers.se.
*E-mail: rupert.huber@ur.de.

ORCID

Philipp Steinleitner: 0000-0001-6808-5547
Kenji Watanabe: 0000-0003-3701-8119
Samuel Brem: 0000-0001-8823-1302
Malte Selig: 0000-0003-0022-412X

Notes

The authors declare no competing financial interest.

■ ACKNOWLEDGMENTS

The authors thank Matthias Knorr for helpful discussions and Martin Furthmeier for technical assistance. The work in Regensburg was supported by the European Research Council through Grant 305003 (QUANTUMsubCYCLE) as well as by the Deutsche Forschungsgemeinschaft (through Grants HU1598/2-1, KO3612/1-1, SFB 1277, projects A05, B05, and B06, and GRK 1570). A.C. gratefully acknowledges funding from the Deutsche Forschungsgemeinschaft through the Emmy Noether Programme (CH1672/1-1). The Chalmers group acknowledges funding from the European Union's Horizon 2020 research and innovation program under Grant Agreement 696656 (Graphene Flagship) and the Swedish Research Council (VR). The Berlin group was supported by the Deutsche Forschungsgemeinschaft (DFG) through the collaborative research centers SFB 787 and 951. K.W. and T.T. acknowledge support from the Elemental Strategy Initiative conducted by the MEXT, Japan and JSPS KAKENHI Grant JP15K21722.

■ REFERENCES

(1) Splendiani, A.; Sun, L.; Zhang, Y.; Li, T.; Kim, J.; Chim, C.-Y.; Galli, G.; Wang, F. Emerging Photoluminescence in Monolayer MoS_2. *Nano Lett.* **2010**, *10*, 1271−1275.

(2) Mak, K. F.; Lee, C.; Hone, J.; Shan, J.; Heinz, T. F. Atomically Thin MoS_2: A New Direct-Gap Semiconductor. *Phys. Rev. Lett.* **2010**, *105*, 136805.

(3) Wang, Q. H.; Kalantar-Zadeh, K.; Kis, A.; Coleman, J. N.; Strano, M. S. Electronics and optoelectronics of two-dimensional transition metal dichalcogenides. *Nat. Nanotechnol.* **2012**, *7*, 699−712.

(4) Britnell, L.; Ribeiro, R. M.; Eckmann, A.; Jalil, R.; Belle, B. D.; Mishchenko, A.; Kim, Y.-J.; Gorbachev, R. V.; Georgiou, T.; Morozov, S. V.; et al. Strong Light-Matter Interactions in Heterostructures of Atomically Thin Films. *Science* **2013**, *340*, 1311−1314.

(5) Ross, J. S.; Klement, P.; Jones, A. M.; Ghimire, N. J.; Yan, J.; Mandrus, D. G.; Taniguchi, T.; Watanabe, K.; Kitamura, K.; Yao, W.; Cobden, D. H.; Xu, X. Electrically tunable excitonic light-emitting diodes based on monolayer WSe_2 p−n junctions. *Nat. Nanotechnol.* **2014**, *9*, 268−272.

(6) Ramasubramaniam, A. Large excitonic effects in monolayers of molybdenum and tungsten dichalcogenides. *Phys. Rev. B: Condens. Matter Mater. Phys.* **2012**, *86*, 115409.

(7) He, K.; Kumar, N.; Zhao, L.; Wang, Z.; Mak, K. F.; Zhao, H.; Shan, J. Tightly Bound Excitons in Monolayer WSe_2. *Phys. Rev. Lett.* **2014**, *113*, 026803.

(8) Berkelbach, T. C.; Hybertsen, M. S.; Reichman, D. R. Theory of neutral and charged excitons in monolayer transition metal

DOI: 10.1021/acs.nanolett.7b05132
Nano Lett. XXXX, XXX, XXX−XXX

dichalcogenides. *Phys. Rev. B: Condens. Matter Mater. Phys.* **2013**, *88*, 045318.
(9) Berghäuser, G.; Malic, E. Analytical approach to excitonic properties of MoS_2. *Phys. Rev. B: Condens. Matter Mater. Phys.* **2014**, *89*, 125309.
(10) Ye, Z.; Cao, T.; O'Brien, K.; Zhu, H.; Yin, X.; Wang, Y.; Louie, S. G.; Zhang, X. Probing excitonic dark states in single-layer tungsten disulphide. *Nature* **2014**, *513*, 214−218.
(11) Chernikov, A.; Berkelbach, T. C.; Hill, H. M.; Rigosi, A.; Li, Y.; Aslan, O. B.; Reichman, D. R.; Hybertsen, M. S.; Heinz, T. F. Exciton Binding Energy and Nonhydrogenic Rydberg Series in Monolayer WS_2. *Phys. Rev. Lett.* **2014**, *113*, 076802.
(12) Poellmann, C.; Steinleitner, P.; Leierseder, U.; Nagler, P.; Plechinger, G.; Porer, M.; Bratschitsch, R.; Schüller, C.; Korn, T.; Huber, R. Resonant internal quantum transitions and femtosecond radiative decay of excitons in monolayer WSe_2. *Nat. Mater.* **2015**, *14*, 889−893.
(13) Steinleitner, P.; Merkl, P.; Nagler, P.; Mornhinweg, J.; Schüller, C.; Korn, T.; Chernikov, A.; Huber, R. Direct Observation of Ultrafast Exciton Formation in a Monolayer of WSe_2. *Nano Lett.* **2017**, *17*, 1455−1460.
(14) Cudazzo, P.; Tokatly, I. V.; Rubio, A. Dielectric screening in two-dimensional insulators: Implications for excitonic and impurity states in graphane. *Phys. Rev. B: Condens. Matter Mater. Phys.* **2011**, *84*, 085406.
(15) Fang, H.; Battaglia, C.; Carraro, C.; Nemsak, S.; Ozdol, B.; Kang, J. S.; Bechtel, H. A.; Desai, S. B.; Kronast, F.; Unal, A. A.; et al. Strong interlayer coupling in van der Waals heterostructures built from single-layer chalcogenides. *Proc. Natl. Acad. Sci. U. S. A.* **2014**, *111*, 6198−6202.
(16) Ugeda, M. M.; Bradley, A. J.; Shi, S.-F.; Da Jornada, F. H.; Zhang, Y.; Qiu, D. Y.; Ruan, W.; Mo, S.-K.; Hussain, Z.; Shen, Z.-X.; et al. Giant bandgap renormalization and excitonic effects in a monolayer transition metal dichalcogenide semiconductor. *Nat. Mater.* **2014**, *13*, 1091−1095.
(17) Rösner, M.; Steinke, C.; Lorke, M.; Gies, C.; Jahnke, F.; Wehling, T. O. Two-Dimensional Heterojunctions from Nonlocal Manipulations of the Interactions. *Nano Lett.* **2016**, *16*, 2322−2327.
(18) Stier, A. V.; Wilson, N. P.; Clark, G.; Xu, X.; Crooker, S. A. Probing the Influence of Dielectric Environment on Excitons in Monolayer WSe_2: Insight from High Magnetic Fields. *Nano Lett.* **2016**, *16*, 7054−7060.
(19) Cadiz, F.; Courtade, E.; Robert, C.; Wang, G.; Shen, Y.; Cai, H.; Taniguchi, T.; Watanabe, K.; Carrere, H.; Lagarde, D.; et al. Excitonic Linewidth Approaching the Homogeneous Limit in MoS_2-Based van der Waals Heterostructures. *Phys. Rev. X* **2017**, *7*, 021026.
(20) Raja, A.; Chaves, A.; Yu, J.; Arefe, G.; Hill, H. M.; Rigosi, A. F.; Berkelbach, T. C.; Nagler, P.; Schüller, C.; Korn, T.; et al. Coulomb engineering of the bandgap and excitons in two-dimensional materials. *Nat. Commun.* **2017**, *8*, 15251.
(21) Borghardt, S.; Tu, J.-S.; Winkler, F.; Schubert, J.; Zander, W.; Leosson, K.; Kardynał, B. E. Engineering of optical and electronic band gaps in transition metal dichalcogenide monolayers through external dielectric screening. *Phys. Rev. Mater.* **2017**, *1*, 054001.
(22) Ajayi, O. A.; Ardelean, J. V.; Shepard, G. D.; Wang, J.; Antony, A.; Taniguchi, T.; Watanabe, K.; Heinz, T. F.; Strauf, S.; Zhu, X.-Y.; et al. Approaching the Intrinsic Photoluminescence Linewidth in Transition Metal Dichalcogenide Monolayers. *2D Mater.* **2017**, *4*, 031011.
(23) Geim, A. K.; Grigorieva, I. V. Van der Waals heterostructures. *Nature* **2013**, *499*, 419−425.
(24) Rivera, P.; Schaibley, J. R.; Jones, A. M.; Ross, J. S.; Wu, S.; Aivazian, G.; Klement, P.; Seyler, K.; Clark, G.; Ghimire, N. J.; et al. Observation of long-lived interlayer excitons in monolayer $MoSe_2$-WSe_2 heterostructures. *Nat. Commun.* **2015**, *6*, 6242.
(25) Dufferwiel, S.; Schwarz, S.; Withers, F.; Trichet, A. A. P.; Li, F.; Sich, M.; Del Pozo-Zamudio, O.; Clark, C.; Nalitov, A.; Solnyshkov, D. D.; et al. Exciton-polaritons in van der Waals heterostructures embedded in tunable microcavities. *Nat. Commun.* **2015**, *6*, 8579.
(26) Chen, H.; Wen, X.; Zhang, J.; Wu, T.; Gong, Y.; Zhang, X.; Yuan, J.; Yi, C.; Lou, J.; Ajayan, P. M.; et al. Ultrafast formation of interlayer hot excitons in atomically thin MoS_2/WS_2 heterostructures. *Nat. Commun.* **2016**, *7*, 12512.
(27) Rivera, P.; Seyler, K. L.; Yu, H.; Schaibley, J. R.; Yan, J.; Mandrus, D. G.; Yao, W.; Xu, X. Valley-polarized exciton dynamics in a 2D semiconductor heterostructure. *Science* **2016**, *351*, 688−691.
(28) Raja, A.; Montoya-Castillo, A.; Zultak, J.; Zhang, X.-X.; Ye, Z.; Roquelet, C.; Chenet, D. A.; Van der Zande, A. M.; Huang, P.; Jockusch, S.; et al. Energy Transfer from Quantum Dots to Graphene and MoS_2: The Role of Absorption and Screening in Two-Dimensional Materials. *Nano Lett.* **2016**, *16*, 2328−2333.
(29) Hill, H. M.; Rigosi, A. F.; Rim, K. T.; Flynn, G. W.; Heinz, T. F. Band Alignment in MoS_2/WS_2 Transition Metal Dichalcogenide Heterostructures Probed by Scanning Tunneling Microscopy and Spectroscopy. *Nano Lett.* **2016**, *16*, 4831−4837.
(30) Jin, C.; Kim, J.; Suh, J.; Shi, Z.; Chen, B.; Fan, X.; Kam, M.; Watanabe, K.; Taniguchi, T.; Tongay, S.; et al. Interlayer electron-phonon coupling inWSe_2/hBN heterostructures. *Nat. Phys.* **2017**, *13*, 127−131.
(31) Chow, C. M.; Yu, H.; Jones, A. M.; Yan, J.; Mandrus, D. G.; Taniguchi, T.; Watanabe, K.; Yao, W.; Xu, X. Unusual Exciton-Phonon Interactions at van der Waals Engineered Interfaces. *Nano Lett.* **2017**, *17*, 1194−1199.
(32) Manca, M.; Glazov, M. M.; Robert, C.; Cadiz, F.; Taniguchi, T.; Watanabe, K.; Courtade, E.; Amand, T.; Renucci, P.; Marie, X.; et al. Enabling valley selective exciton scattering in monolayer WSe_2 through upconversion. *Nat. Commun.* **2017**, *8*, 14927.
(33) Lee, C.-H.; Lee, G.-H.; Van der Zande, A. M.; Chen, W.; Li, Y.; Han, M.; Cui, X.; Arefe, G.; Nuckolls, C.; Heinz, T. F.; et al. Atomically thin p−n junctions with van der Waals heterointerfaces. *Nat. Nanotechnol.* **2014**, *9*, 676−681.
(34) Withers, F.; Del Pozo-Zamudio, O.; Mishchenko, A.; Rooney, A. P.; Gholinia, A.; Watanabe, K.; Taniguchi, T.; Haigh, S. J.; Geim, A. K.; Tartakovskii, A. I.; et al. Light-emitting diodes by band-structure engineering in van der Waals heterostructures. *Nat. Mater.* **2015**, *14*, 301−306.
(35) Rigosi, A. F.; Hill, H. M.; Li, Y.; Chernikov, A.; Heinz, T. F. Probing Interlayer Interactions in Transition Metal Dichalcogenide Heterostructures by Optical Spectroscopy: MoS_2/WS_2 and $MoSe_2/WSe_2$. *Nano Lett.* **2015**, *15*, 5033−5038.
(36) Selig, M.; Berghäuser, G.; Raja, A.; Nagler, P.; Schüller, C.; Heinz, T. F.; Korn, T.; Chernikov, A.; Malic, E.; Knorr, A. Excitonic linewidth and coherence lifetime in monolayer transition metal dichalcogenides. *Nat. Commun.* **2016**, *7*, 13279.
(37) Christiansen, D.; Selig, M.; Berghäuser, G.; Schmidt, R.; Niehues, I.; Schneider, R.; Arora, A.; De Vasconcellos, S. M.; Bratschitsch, R.; Malic, E.; Knorr, A. Phonon Sidebands in Monolayer Transition Metal Dichalcogenides. *Phys. Rev. Lett.* **2017**, *119*, 187402.
(38) Wang, G.; Robert, C.; Glazov, M. M.; Cadiz, F.; Courtade, E.; Amand, T.; Lagarde, D.; Taniguchi, T.; Watanabe, K.; Urbaszek, B.; et al. In-Plane Propagation of Light in Transition Metal Dichalcogenide Monolayers: Optical Selection Rules. *Phys. Rev. Lett.* **2017**, *119*, 047401.
(39) Cha, S.; Sung, J. H.; Sim, S.; Park, J.; Heo, H.; Jo, M.-H.; Choi, H. 1*s*-intraexcitonic dynamics in monolayer MoS_2 probed by ultrafast mid-infrared spectroscopy. *Nat. Commun.* **2016**, *7*, 10768.
(40) Berghäuser, G.; Steinleitner, P.; Merkl, P.; Huber, R.; Knorr, A.; Malic, E. Mapping of the dark exciton landscape in transition metal dichalcogenides. **2017**, arxiv 1708.07725, accessed 1/9/2018.
(41) Castellanos-Gomez, A.; Buscema, M.; Molenaar, R.; Singh, V.; Janssen, L.; Van der Zant, H. S. J.; Steele, G. A. Deterministic transfer of two-dimensional materials by all-dry viscoelastic stamping. *2D Mater.* **2014**, *1*, 011002.
(42) Huber, R.; Tauser, F.; Brodschelm, A.; Bichler, M.; Abstreiter, G.; Leitenstorfer, A. How many-particle interactions develop after ultrafast excitation of an electron-hole plasma. *Nature* **2001**, *414*, 286−289.

DOI: 10.1021/acs.nanolett.7b05132
Nano Lett. XXXX, XXX, XXX−XXX

(43) Kaindl, R. A.; Carnahan, M. A.; Hägele, D.; Lövenich, R.; Chemla, D. S. Ultrafast terahertz probes of transient conducting and insulating phases in an electron-hole gas. *Nature* **2003**, *423*, 734−738.
(44) Kaindl, R. A.; Hägele, D.; Carnahan, M. A.; Chemla, D. S. Transient terahertz spectroscopy of excitons and unbound carriers in quasi-two-dimensional electron-hole gases. *Phys. Rev. B: Condens. Matter Mater. Phys.* **2009**, *79*, 045320.
(45) Ménard, J.-M.; Poellmann, C.; Porer, M.; Leierseder, U.; Galopin, E.; Lemaître, A.; Amo, A.; Bloch, J.; Huber, R. Revealing the dark side of a bright exciton-polariton condensate. *Nat. Commun.* **2014**, *5*, 4648.
(46) Almand-Hunter, A. E.; Li, H.; Cundiff, S. T.; Mootz, M.; Kira, M.; Koch, S. W. Quantum droplets of electrons and holes. *Nature* **2014**, *506*, 471−475.
(47) Selig, M.; Berghäuser, G.; Richter, M.; Bratschitsch, R.; Knorr, A.; Malic, E. Dark and bright exciton formation, thermalization, and photoluminescence in monolayer transition metal dichalcogenides. **2017**, arxiv 1703.03317, accessed 1/9/2018.
(48) Rytova, N. S. Screened potential of a point charge in a thin film. *Mosc. Univ. Phys. Bull.* **1967**, *3*, 30.
(49) Keldysh, L. V. Coulomb interaction in thin semiconductor and semimetal films. *JETP Lett.* **1979**, *29*, 658−661.
(50) Kim, K. K.; Hsu, A.; Jia, X.; Kim, S. M.; Shi, Y.; Dresselhaus, M.; Palacios, T.; Kong, J. Synthesis and Characterization of Hexagonal Boron Nitride Film as a Dielectric Layer for Graphene Devices. *ACS Nano* **2012**, *6*, 8583−8590.

DOI: 10.1021/acs.nanolett.7b05132
Nano Lett. XXXX, XXX, XXX−XXX